Editors' Suggestion

Tuning domain wall conductivity in bulk lithium niobate by uniaxial stress

Ekta Singh [1,2] Henrik Beccard [1] Zeeshan H. Amber [1] Julius Ratzenberger [1] Clifford W. Hicks [2,3] Michael Rüsing [1] and Lukas M. Eng [1,4]

[1]*Institute of Applied Physics, TU Dresden, Nöthnitzer Straße 61, 01187 Dresden, Germany*
[2]*Max Planck Institute for Chemical Physics of Solids, Nöthnitzer Straße 40, 01187 Dresden, Germany*
[3]*School of Physics and Astronomy, University of Birmingham, Birmingham B15 2TT, United Kingdom*
[4]*ct.qmat: Dresden-Würzburg Cluster of Excellence-EXC 2147, TU Dresden, 01062 Dresden, Germany*

(Received 24 May 2022; revised 27 August 2022; accepted 29 August 2022; published 19 October 2022)

Conductive domain walls (DWs) in insulating ferroelectrics have recently attracted considerable attention due to their unique topological, optical, and electronic properties, and offer potential applications such as in memory devices or rewritable circuitry. The electronic properties of DWs can be tuned by the application of strain, hence controlling the charge carrier density at DWs. In this paper, we study the influence of uniaxial stress on the conductivity of DWs in the bulk single crystal lithium niobate ($LiNbO_3$). Using conductive atomic force microscopy, we observe a large asymmetry in the conductivity of DWs, where only negatively screened walls, so called head-to-head DWs, are becoming increasingly conductive, while positively screened, tail-to-tails DWs, show a decrease in conductivity. This asymmetry of DW conductivity agrees with our theoretical model based on the piezoelectric effect. In addition, we observed that the current in the DW increases up to an order of magnitude for smaller compressive stresses of 100 MPa. This response of DWs remained intact for multiple stress cycles over two months, opening a path for future applications.

DOI: 10.1103/PhysRevB.106.144103

I. INTRODUCTION

For the last decade, ferroelectric domain walls (DWs) have been in the focus of research due to their outstanding optical, electrical, and topological properties that promise numerous applications such as resistive switches and nonvolatile ferroelectric memory devices [1–3]. These applications take advantage of conductive nature of ferroelectric DWs, where on and off states of the devices can be defined by the resistance of DWs [2,4–8]. In most models, the conductivity of DWs is connected to the order parameter of the surrounding domains, which for ferroelectrics is the spontaneous polarization P_s. In the context of conductivity, three main configurations of a DW are distinguished:

(1) Neutral DWs: When P_s from neighboring domains are aligned antiparallel to each other as depicted in Fig. 1(a).

(2) Head-to-head (h2h) DWs: When P_s from different domains meet at their positive ends.

(3) Tail-to-tail (t2t) DWs, which are the opposing configuration of h2h, see Fig. 1(b).

The convergence of polarization in cases (2) and (3) creates nonzero bound surface charges localized at the DW, which becomes a source of the so-called depolarization field. This field is then compensated by mobile screening charge carriers such as electrons, holes, polarons, or mobile ions. In some cases, the depolarization field is even strong enough ($\approx$1 MV/cm) to locally bend the conduction band below the Fermi level, hence creating a 2D electron gas at the DW, which, for example, was reported in $BaTiO_3$ [9,10]. The presence of such charged CDWs is reported for many ferroelectrics such as $BiFeO_3$ [11,12], $PbTiO_3$ [13], $BaTiO_3$ [14], $HoMnO_3$ [15], $LiNbO_3$ [16–18], etc. In ferroelectrics, DWs can be easily written, erased, moved, or even switched between different states of conductivity. The most common method is by the application of electric fields. Electric fields are able to create or erase DWs via ferroelectric poling. In the case of $LiNbO_3$, it further allows us to control the amount of charge accumulation, e.g., by controlling the tilt angle of the DW with respect to the polar axis [4,19,20]. The control of charge accumulation or, in other words, the conductivity of DWs, allows us to enlarge the memory window for ferroelectric-based memory devices [4]. Another elegant possibility to control and study the accumulation of bound charges is via direct piezoelectricity [21,22], i.e., by inducing an additional polarization component through stress or strain [see Fig. 1(c)], which so far has only been reported for a few selected materials. For example, Ederer and Spaldin evaluated the effect of epitaxial strain of up to $\pm$2.5% on the spontaneous polarization (P_s) for different ferroelectrics [23]. Experimentally, Chen *et al.* measured the spontaneous polarization and conductivity of DWs of strained $BiFO_3$ thin films. They reported that strain tuning changes the DW conductivity by several orders of magnitude indicating effects not just due to screening charges but band bending as well [24]. In the reported experimental

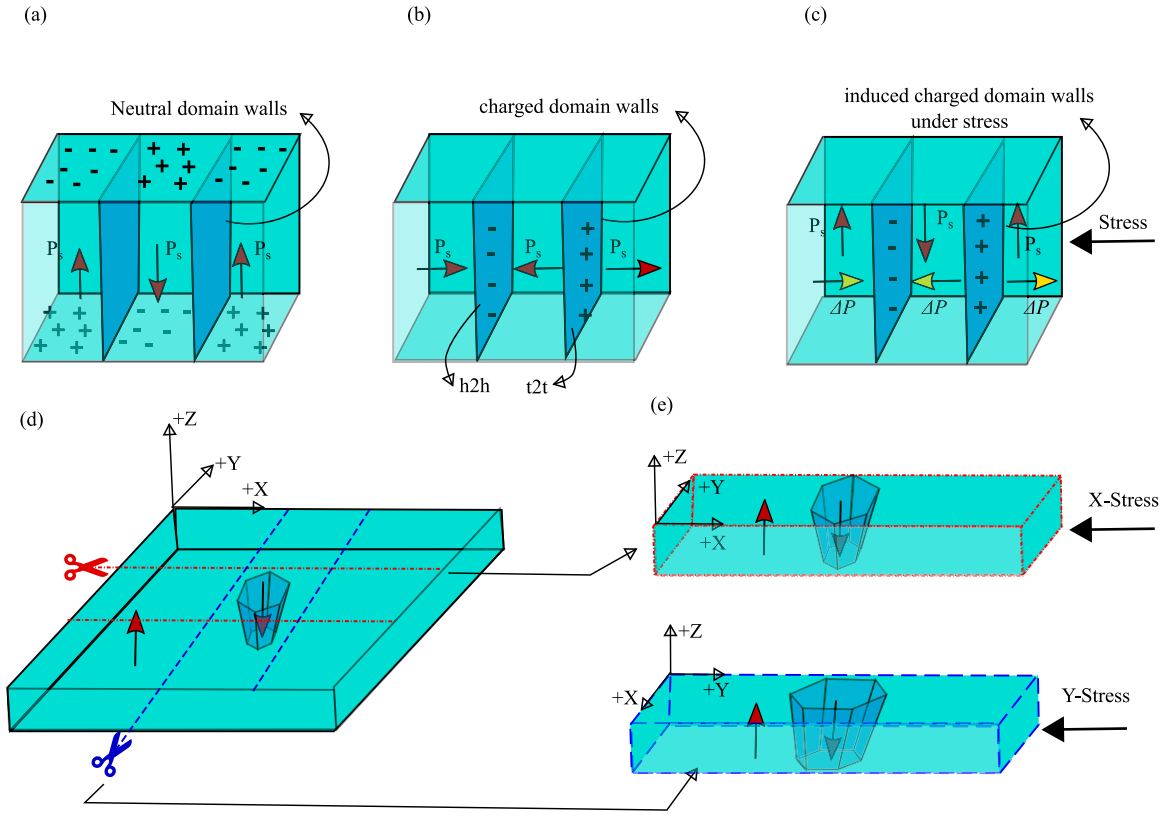

FIG. 1. Sketch: (a) Neutral domain walls in a ferroelectric, where red arrows are representing the spontaneous polarization parallel to domain walls. (b) Charged domain walls: Spontaneous polarizations meet head-to-head (h2h) and tail-to-tail (t2t) perpendicular to domain walls. (c) Neutral domain walls but charged due to induced polarization, represented by yellow arrows, when stress is applied to a crystal. Charges shown in the images are screening charge carriers. (d) Piece of single crystal Z-cut $LiNbO_3$ containing a hexagonal domain. (e) Two different $LiNbO_3$ samples cut along different axes from the parent crystal in image (d). The samples are cut such that stress can be applied to the crystallographic *x* and *y* axes.

or theoretical cases, the application and amount of strain is limited by lattice-mismatched epitaxial growth of thin films on specifically selected substrates and, therefore, cannot be generalized to all ferroelectric materials or crystallographic orientations [25].

To enable the study of strain on the DW conductivity for any bulk ferroelectric, we report the room-temperature DW conductivity of $LiNbO_3$ under uniaxial stress by combining a *in situ* tunable uniaxial stress cell with scanning probe microscopy. With the help of conductive atomic force microscopy (cAFM), we show the local change of the current distribution in DWs, when stress is applied along different crystallographic directions in $LiNbO_3$. The experimental results are readily explained with our model based on the direct piezoelectric effect in $LiNbO_3$.

For our study, we have chosen the ferroelectric material lithium niobate (5% MgO-doped $LiNbO_3$), where highly CDWs with currents of up to $\approx$1 mA at 10 V in 200-μm-thick crystals have been reported [1,19]. Recent experiments in LNO have demonstrated that DWs can be switched between conductive and nonconductive states with a memory window of $>10^4$ via electric fields in both thin films and bulk devices [1,4]. This switching process can be used for fabricating a two-terminal memory device with an extrapolated 80% lifetime of $>$10 years [4]. Therefore, $LiNbO_3$ is an ideal model system to study the effects of strain on DW conductivity.

II. EXPERIMENTAL METHODS

Conductive atomic force microscopy measurements were performed under uniaxial stress to see the local effects of stress at $LiNbO_3$ CDWs. For this measurement, we have used the uniaxial stress cell as shown in Fig. 2. In this design, a central piezoelectric stack, connected to the main body of the cell, applies compressive stress, while the outer stacks apply tensile stress [26], see Fig. 2(a). Mechanically, the cell is composed of two different parts A and B of different spring constants which are then connected by the sample in mechanical series, as shown in Fig. 2(b). Being in series, all parts along with the sample experience the same force but different stresses. This force on the cell is measured by a force sensor placed at the end of device, which consists of four strain gauges mounted in a Wheatstone bridge configuration. The cell is controlled by a feedback loop written in Python.

The samples used are single-crystal Z-cut 5% MgO-doped $LiNbO_3$ (LNO) obtained from Yamaju Ceramics Co., Ltd. The domains in the crystal were subsequently written by the UV-assisted poling method [27]. In this method, the sample is fixed in between two small O rings, which themselves are confined in a cell. The cell is then filled with water. The water acts as a uniform top and bottom contact to the sample. A DC voltage is applied to the water using conductive wires. The cell consists of quartz glass which allows a UV laser of 325 nm

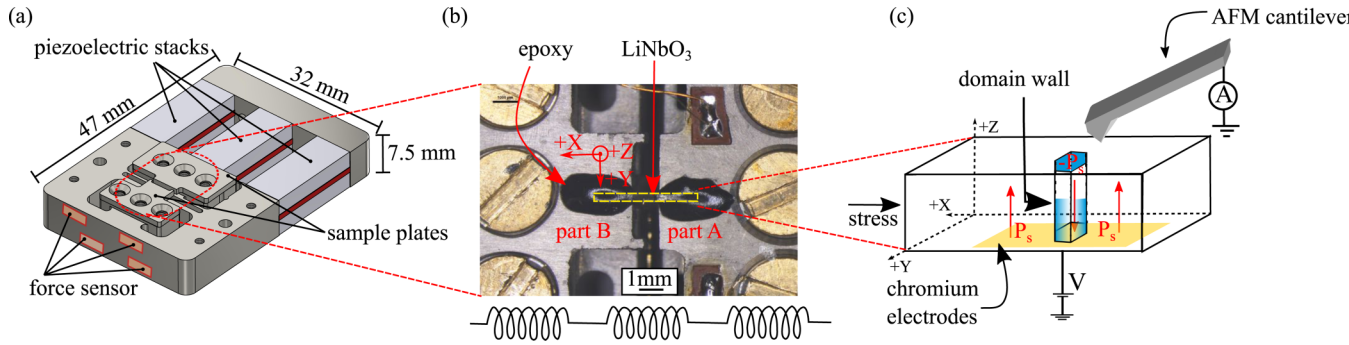

FIG. 2. (a) Three-dimensional sketch of the uniaxial stress cell. (b) Zoom-in image of the stress cell: Z-cut 5% MgO-doped $LiNbO_3$ (sample: LNO-01) mounted on the cell with 2850FT epoxy. (c) Sketch of the setup for cAFM measurement with applied stress. Domains and domain walls are electrically connected by a 20-nm-thick chromium electrode at the $-z$ side and grounded by the cantilever at the $+z$ side.

wavelength (λ) to enter it. The laser is focused on the sample, which locally decreases the coercive field (E_c) of $LiNbO_3$ [28]; as a result, the electric dipoles first start to flip locally or, in other words, the nucleation of the domain takes place. If the electric field is removed faster from the sample, the dipoles can switch back. This way the nested domain can be written in a user-defined area of a crystal as shown in Figs. 4(a) and 6(a).

Here, we analyzed two samples, which are prepared such that the stress can be applied along different crystal axes [see Figs. 1(d) and 1(e)]. Sample LNO-01 with a cross section of 310 μm$\times$200 μm ($z\times y$) is compressed along the crystallographic x axis, while sample LNO-02 with the cross section 370 μm$\times$200 μm ($z\times x$) is compressed along the crystallographic y axis. Afterward, fabricated domain structures were treated to increase the conductivity by the procedure developed by Godau *et al.* [19]. In the enhancement procedure, the 20-nm-thick chromium electrodes were used to apply ≈ -500 V DC voltage to the $+$Z surface of the 200-μm-thick sample, with this inclination angle of DWs increased by $\sim 1^\circ$ [29] and the current increased by a factor of 10^4 (at -10 V) compared to as-poled DWs (more details are in the Supplemental Material [30] in Sec. S1). The cAFM measurements were performed on the NX10 scanning probe microscope from Park Systems Corp.

Piezoresponse force microscopy (PFM) [31] on the samples was performed using pure platinum tips model RMN-25PT300B (free resonance frequency, $f_{\text{free}} \approx 20$ kHz) as a top contact, while applying the external mechanical stress. For PFM, an alternating voltage of 20 V_{p-p} at a frequency smaller than contact resonance frequency($f_{\text{cont}} \approx 41$ kHz) was applied to the cantilever. cAFM was also performed using the same RMN tips. The sample in this case was kept at -10 V while the cantilever and the stress cell were kept at ground, see Fig. 2(c).

III. THEORETICAL MODEL

The conductivity of ferroelectric DWs in $LiNbO_3$ is believed to be related to the amount of screening charges present at the DW. As shown in Figs. S2 and S3 of the Supplemental Material [30] and discussed in the literature [1,18,19], any increase of the DW inclination angle α, with respect to the polar axis, results in an increase of the screening charge carrier density σ and, ideally, its conductivity by $\sigma = 2P_s \sin\alpha$. Alike, applying stress to the sample results in a change of screening charge carriers by induced polarization through the direct piezoelectric effect. This can be used to predict and describe the behavior of CDWs with respect to applied stress. The polarization ΔP in the crystal of $LiNbO_3$ can be described via

$$\begin{bmatrix} P_x \\ P_y \\ P_z \end{bmatrix} = \begin{bmatrix} 0 & 0 & 0 & 0 & d_{15} & -2d_{22} \\ -d_{22} & d_{22} & 0 & d_{15} & 0 & 0 \\ d_{31} & d_{31} & d_{33} & 0 & 0 & 0 \end{bmatrix} \begin{bmatrix} X_1 \\ X_2 \\ X_3 \\ X_4 \\ X_5 \\ X_6 \end{bmatrix}, \tag{1}$$

where $[d]$ is the matrix of piezoelectric strain coefficients and $[X]$ is the stress matrix [32–34] (details on the calculation and the tensor elements for $LiNbO_3$ are presented in the Supplemental Material Sec. S2 [30]). When the $LiNbO_3$ crystal is stressed along the crystallographic x axis as in the sample LNO-01 which we have measured in this work, an extra polarization is induced along both the y and z axes, as provided in Fig. 3(a). The values of induced polarizations along the y axis ($\Delta P_y = 0.208\times10^{-2}$ Cm^{-2}) and the z axis ($\Delta P_z = 0.863\times10^{-4}$ Cm^{-2}) for a compressive stress of -100 MPa are significantly smaller than the spontaneous polarization of $LiNbO_3$ ($P_s \approx 0.7$ Cm^{-2} [35]). However, as the polarization ΔP_y is projected perpendicular to ΔP_z at the DW, it contributes as a cosine component to the surface charge density equation and results in a significant surface charge density (σ) at the DWs ($\Delta\sigma_y + \Delta\sigma_z = 2\Delta P_y \cos\alpha + 2\Delta P_z \sin\alpha$), as depicted by the sketches in Fig. 3(a). This is in the same order of magnitude as the natural charge density σ for small angles of inclination of $\alpha = 1^\circ$, typically observed for enhanced DWs [19]. As a result, x-compressed DWs, which are oriented at some angle to the y axis, should become h2h or t2t like, and thus should be screened additionally by negative or positive mobile charge carriers, respectively. Depending on their geometry, from now on we will refer to them as induced h2h, i(h2h) and induced t2t, i(t2t) DWs.

Since $LiNbO_3$ is piezoelectric along the y axis, one should expect exactly the opposite behavior when the sample is compressed along that crystallographic y axis, as we will indeed report below for sample LNO-02. This happens due to the sign

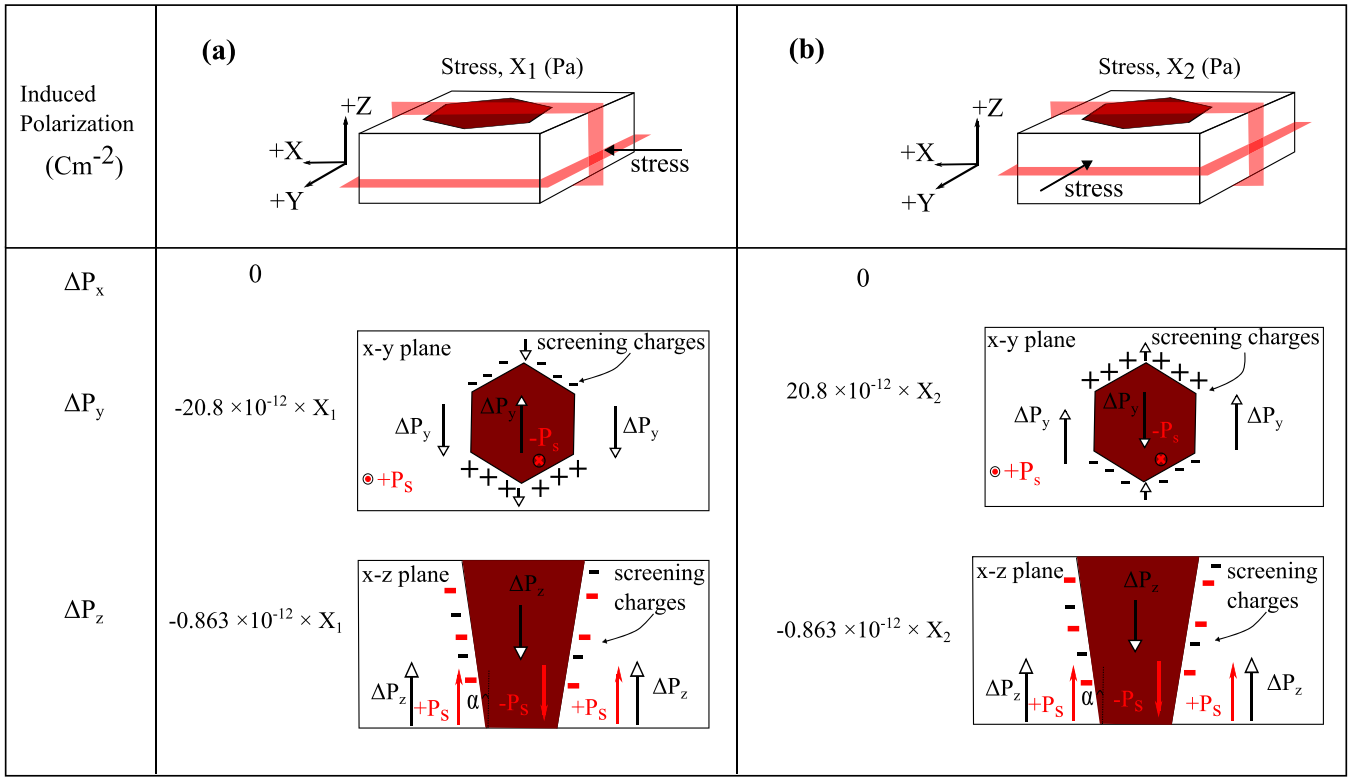

FIG. 3. Projection of induced polarization ($P_j = d_{jkl}X_{kl}$) at DWs along different axes at zero external electric field when $LiNbO_3$ is stressed along (a) x axis and (b) y axis, where for $LiNbO_3$, $d_{22} = 20.8\times10^{-12}$ C/N and $d_{31} = -0.863\times10^{-12}$ C/N at room temperature [32]. The sign of stress should be negative for compression and positive for tension. Each sketch belongs to the respective column above depicts directions of induced polarization at DWs for compression configuration. The directions should be reversed for tension. Charges shown at DWs are screening charges, which are responsible for the conductivity in DWs (detailed calculations are given in the Supplemental Material [30]).

inversion of d_{22} in Eq. (1). This is depicted in Fig. 3(b). In a y-compression scenario, the induced polarization ΔP_y will change the direction by 180° in contrast to the ΔP_y in x compression, and the DWs which were i(h2h) in x compression will become i(t2t) for y compression.

When applying this model to our LNO-01 and LNO-02 samples, we expect DW currents to behave as described in the sketches of Figs. 4(b), 4(d) and 6(b). We show that the DWs highlighted in blue-solid lines should become i(h2h) type (negatively screened) while grey dotted DWs should become i(t2t) type (positively screened), and green dashed DWs should not be influenced by uniaxial stress at all. The opposite behavior should be observed under tensile stress.

IV. EXPERIMENTAL RESULTS

To locate the domains, PFM was performed on the $+z$ side of sample LNO-01, as illustrated in Fig. 4(a). As seen in Fig. 4(c), the PFM image agrees well with SHG imaging and confirms the presence of the same DWs. In the PFM image, the yellow-and-black color contrast represents a phase difference of 180° between two different orientations, while in SHG microscopy the presence of DWs is indicated by an enhanced backscattered signal. Based on the PFM scans, cAFM was performed at the same location at different stresses while applying a −10 V dc voltage to the bottom contact ($-z$ side). Figure 4(e) shows a cAFM overview at 0 MPa. Here, only parts of the DWs show conductivity. The reason for this could be different near surface inclination angles of DWs, leading to locally different Schottky barriers, which has been reported earlier [15,18–20]. However, the observed locations correspond to the shape and location of the DWs as observed in PFM and SHG microscopy.

When compressing the sample along the x axis, we expect the DWs with i(h2h) and i(t2t) configurations to be additionally charged. The i(h2h) DWs must get more conductive because the amount of negative screening charges increases. On the other hand, i(t2t) DWs first should fully compensate the preexisting negative screening charges at the DW. This means for i(t2t) DWs that the current should first reduce to zero and on application of further compressive stress, one should expect these i(t2t) DWs to become conductive again. Both types of DWs are highlighted by blue-solid and grey-dotted lines in the sketch in Fig. 4(b). The image in Fig. 4(f) below shows a cAFM scan taken at −129 MPa. Indeed, we see an enhanced conductivity for the i(h2h) configurations, while the i(t2t) walls are observed to show a decreasing conductivity. When the compression is relaxed back to 0 MPa again, as depicted in Fig. 4(g), it retains a qualitatively similar picture to the initial state [Fig. 4(e)]. When tensile stress is applied, only the walls with a i(h2h) configuration with respect to the induced polarization exhibit a significant increased conductivity, while the induced i(t2t) DWs show a disappearing conductivity as shown in Figs. 4(d) and 4(h). In all cases, the neutral walls with respect to the induced polarization show similar qualitative behavior. Although, weak and less strict

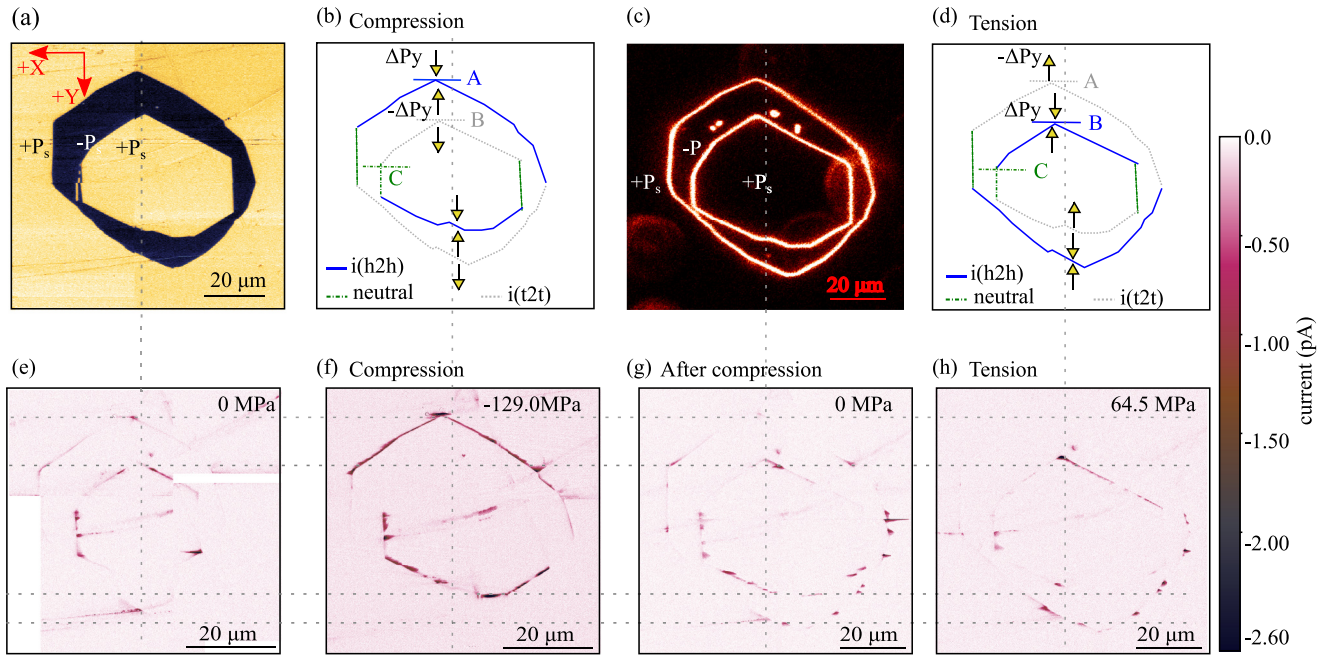

FIG. 4. (a) Stitched PFM phase image of LNO-01 sample (x compression), arrows on top left shows crystallographic axes. (b) Current distribution in DWs under compressive stress according to a model based on direct piezoelectricity. (c) SHG image of LNO sample. (d) Current distribution of DWs under tensile stress according to a model based on direct piezoelectricity. Stitched cAFM image of DWs: (e) at 0 MPa stress, (f) at −129.0 MPa compressive stress, (g) at 0 MPa after compression, and (h) at 64.5 MPa tensile stress. The DWs in (f) and (h) show expected response as in sketches above them, (b) and (d), respectively.

current fluctuations can be observed at different stress values. In an ideal case, when the domain walls are perfectly parallel to the crystallographic y axis all the way through the thickness of the crystal, according to our model the domain wall conductivity should not change. However, in samples LNO-01 and LNO-02, the 3D second harmonic generation (SHG) images in Figs. S5(c) and S4(c) of the Supplemental Materian [30] shows that the DWs along the y axis are not perfectly parallel to the y axis all the way through the thickness of the sample. We suspect this may cause the slight fluctuations of the current in these walls, and because these walls do not show the strict behavior as the domain walls of i(h2h) or (it2t) type, we categorized them as neutral DWs based on our model.

Additional experiments were performed in intermediate steps of approximately 16.12 MPa for both tension and compression in the range from −129 MPa (compression) up to +64.5 MPa (tensile), as well as repeated multiple times. Selected results can be found in Fig. S6 of the Supplemental Material Sec. S3.1 [30]. In all cases, similar qualitative and quantitative results were obtained as expected, where only the i(h2h) DWs show a significant contribution to the conductivity. To verify whether the conductivity of the DWs changes with time, we measured short-term and long-term time dependence on the sample LNO-01. In the short-term measurement, the sample was kept at −129.0 MPa and the cAFM scans were performed for more than an hour (see Figs. S9 and S10 of the Supplemental Material [30]). As a result, no significant change in the conductivity was observed. On the other hand, in the long-term measurement, the sample was compressed and relaxed over two months. The cAFM measurements were taken in both compressed and relaxed states. The qualitative response of the DW conductivity remained intact. However, a decrease in the overall DW conductivity was observed.

The observation that only h2h DWs exhibit a high electric conductivity has been reported before for $LiNbO_3$ and other ferroelectrics for tilted DWs, and can be explained by the proposed microscopic mechanism of DW conductivity. For $LiNbO_3$, the DW conductivity is explained by hopping transport of electrons in bound-polaronic states, while hole polarons are expected to be only a weak contributor. Hence, only h2h, i.e., negatively screened walls, will contribute to overall conductivity. In this regard, our experiment is in agreement with the polaron-hopping transport mechanism [36]. Based on the piezoelectric theory, the induced polarization is directly proportional to the applied stress. Hence, the conductivity for h2h walls should increase approximately linear with increasing polarization. To show the change in the current as a function of stress more clearly, we have plotted in Fig. 5 the maximum current from line profiles A–C [taken from i(h2h), i(t2t) and neutral parts of DWs in Fig. 4, respectively]. This graph shows three different kinds of behavior:

(1) The DW depicted along the line profile A shows an increase in conductivity on compression, while it shows almost no response for tensile stress within the resolution limit of our setup.

(2) In contrast, the DW in profile B shows the opposite response, as this wall gets an induced i(h2h) configuration for tensile stress. On the other hand:

(3) The DW in line profile C shows no distinctive behavior.

It should be noted that in this experiment, additional to the effects of induced polarizations ΔP_y and ΔP_z, we also expect to see effects from local roughness and local inclinations of

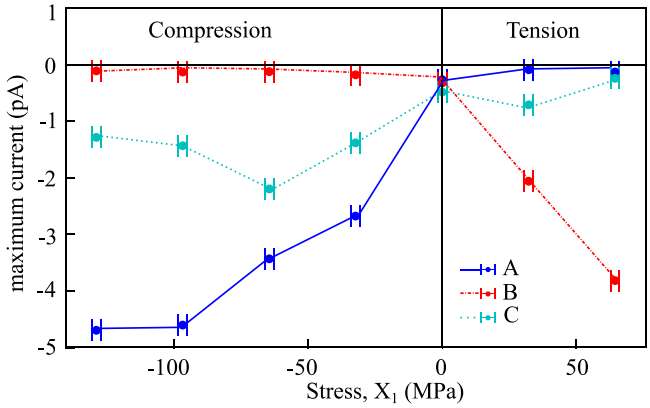

FIG. 5. Change in current with stress along the line profiles A–C taken from different sections of DWs of sample LNO-01(x compression), provided in Figs. 4(b) and 4(d).

the DWs. Therefore, charge carriers inside the crystal might not move in a simple path vertically along the DWs and therefore distorting the ideally expected linear relationships. Effects like this may be predicted based on a resistor network model of DWs [37] in future work.

Apart from the cAFM studies on the sample LNO-01, we have also investigated the response of the DWs to stress with large, deposited electrodes covering all the DWs. These electrodes were the same that were also used for the enhancement procedure. In this macroscopic picture, we see an overall increase in conductivity with applied stress similar to Fig. 4, line profile A for LNO-01. This is in agreement with the fact that in this specific sample the i(h2h) DWs dominate the conductivity. However, it should be noted that this result may not be generalized to all samples and will depend on which induced domain type dominates [i(h2h) or i(t2t)] the conductivity, as was observed for sample LNO-02 (details of the macroscopic curve for both samples are provided in Figs. S2 and S3 of the Supplemental Material Sec. S1.1 [30]). Therefore, this retrospectively motivates the microscopic cAFM study.

For a sample compressed along the y axis, a different behavior from x-axis compression according to the model is expected. Hence, when a similar cAFM measurement was performed on sample LNO-02, we observed the opposite response, as explained by the theoretical model in last section. Figure 6(a) represents the PFM image taken on $+z$ surface. The DWs in sample LNO-02 are more conductive by factor of 3 even at 0 MPa, as compared to sample LNO-01 as shown by Fig. 6(c). This is due to the inclination angle α of DWs in LNO-02 being more than in LNO-01 by 1°, see angle calculation in Figs. S4 and S5 of Supplemental Material Sec. S1.2 [30]. In Figs. 6(c) and 6(d), we only show the cAFM image of the outer wall in the sample LNO-02. The inner domain has an irregular shape and the irregularities in terms of the distance are very close to each other [see Fig. 6(a)]. When cAFM was performed on this domain wall at 0 MPa (unstressed state), the smearing of the current made locating the inner DW difficult. On the application of stress, the same smearing also caused the analysis impossible. Therefore, to keep the explanation clear and understandable, we do not show the inner domain wall. Nevertheless, when compressive stress of −300.6 MPa was

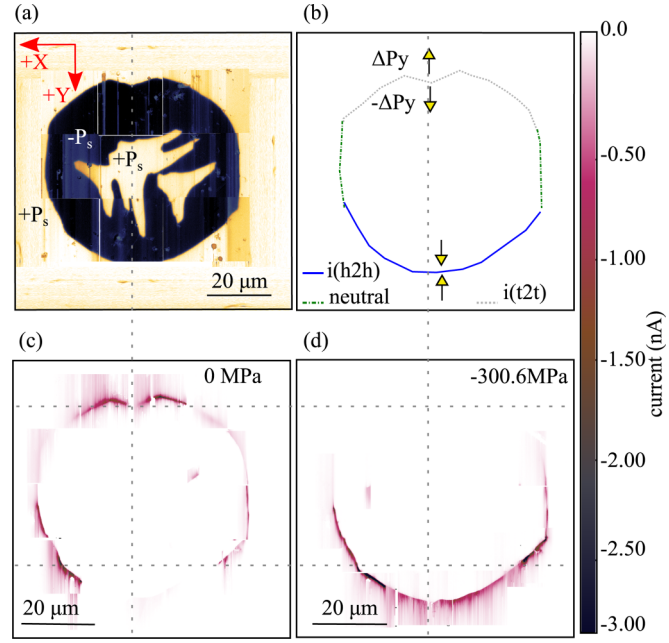

FIG. 6. (a) Stitched PFM phase image of LNO-02 sample (y compression). Arrows on top left show crystallographic axes. (b) Current distribution in DWs under compressive stress according to a model based on direct piezoelectricity predicts opposite response to the sample LNO-01. Stitched cAFM image of DWs: (c) at 0 MPa stress, (d) at −300.6 MPa compressive stress.

applied along the y axis, the outer walls along the $+y$ direction of the crystal becomes i(h2h) and hence more conductive which is opposite to the response of sample LNO-01 as shown by in Fig. 6(d).

(Further information on sample LNO-02 can be found in the Supplemental Material [30]).

V. CONCLUSION

In summary, we demonstrate that uniaxial compressive or tensile stress along the x and y axes can be used to purposely tune the conductivity of ferroelectric DWs in $LiNbO_3$. Here, applying uniaxial stress to a sample results in a change of screening charges on the domain boundary due to the piezoelectric effect. Depending on the relative orientations of the stress and the DW respectively, a DW can deliberately be configured h2h or t2t, for example. Based on this, our results show that the conductivity is approximately proportional to the amount of induced negative screening charges, i.e., i(h2h) configurations, while induced positively charged walls, i.e., i(t2t) configurations, show a rapid decrease in overall conductivity down to bulk conductivity. This observation hints toward electron polarons, rather than hole polarons, that are the main contributor to the conductivity of DWs in $LiNbO_3$ [38]. The same behavior was observed when measurements were repeated many times over a period of two months (see Supplemental Material Sec. S3.2 [30]). Our measurements were performed on a stress cell that allows us to control uniaxial stress independent of a substrate or temperature and, therefore, offering large flexibility for studying different geometries or materials. In conclusion, with uniaxial stress we

can gain a directional control of DW conductivity, potentially allowing novel applications such as stress- or strain-based nanosensors, as well as providing fundamental insights into the properties of DWs.

ACKNOWLEDGMENTS

We express our great gratitude for financial support by the Deutsche Forschungsgemeinschaft (DFG) through joint DFG-ANR project TOPELEC (No. EN-434/41-1 and No. ANR-18-CE92-0052), the CRC1143 (ID No. 247310070), the FOR5044 (ID No. 426703838) [39], as well as by the Würzburg-Dresden Cluster of Excellence on Complexity and Topology in Quantum Matter–ct.qmat (EXC 2147; ID No. 39085490). We also acknowledge the excellent support by the Light Microscopy Facility, a Core Facility of the CMCB Technology Platform at TU Dresden, where the SHG analysis was performed and Park Systems, on which the cAFM measurements were performed. Furthermore, we thank D. Bieberstein and T. Gemming from IFW Dresden for assistance with dicing of the wafers, Dr. Elke Beyreuther for valuable discussions, and Ahmed Samir Lotfy for his laboratory assistance to this work. Ekta Singh acknowledges support from the International Max Planck Research School for Chemistry and Physics of Quantum Materials.

[1] B. Kirbus, C. Godau, L. Wehmeier, H. Beccard, E. Beyreuther, A. Haußmann, and L. M. Eng, Real-time 3D imaging of nanoscale ferroelectric domain wall dynamics in lithium niobate single crystals under electric stimuli: implications for domain-wall-based nanoelectronic devices, ACS Appl. Nano Mater. **2**, 5787 (2019).

[2] P. Sharma, Q. Zhang, D. Sando, C. H. Lei, Y. Liu, J. Li, V. Nagarajan, and J. Seidel, Nonvolatile ferroelectric domain wall memory, Sci. Adv. **3**, e1700512 (2017).

[3] J. Zhao, C. Ma, M. Rüsing, and S. Mookherjea, High Quality Entangled Photon Pair Generation in Periodically Poled Thin-Film Lithium Niobate Waveguides, Phys. Rev. Lett. **124**, 163603 (2020).

[4] T. Kämpfe, B. Wang, A. Haußmann, L.-Q. Chen, and L. M. Eng, Tunable non-volatile memory by conductive ferroelectric domain walls in lithium niobate thin films, Crystals **10**, 804 (2020).

[5] J. Jiang, Z. L. Bai, Z. H. Chen, L. He, D. W. Zhang, Q. H. Zhang, J. A. Shi, M. H. Park, J. F. Scott, C. S. Hwang, and A. Q. Jiang, Temporary formation of highly conducting domain walls for non-destructive read-out of ferroelectric domain-wall resistance switching memories, Nat. Mater. **17**, 49 (2018).

[6] L. Li, J. Britson, J. R. Jokisaari, Y. Zhang, C. Adamo, A. Melville, D. G. Schlom, L. Q. Chen, and X. Pan, Giant resistive switching via control of ferroelectric charged domain walls, Adv. Mater. **28**, 6574 (2016).

[7] A. Gruverman, D. Wu, and J. F. Scott, Piezoresponse Force Microscopy Studies of Switching Behavior of Ferroelectric Capacitors on a 100-ns Time Scale, Phys. Rev. Lett. **100**, 097601 (2008).

[8] G. Catalan, J. Seidel, R. Ramesh, and J. F. Scott, Domain wall nanoelectronics, Rev. Mod. Phys. **84**, 119 (2012).

[9] *Topological Structures in Ferroic Materials*, edited by J. Seidel and D. Walls, Springer Series in Materials Science, Vol. 228 (Springer International Publishing, Cham, 2016), pp. 103–138.

[10] T. Sluka, A. K. Tagantsev, D. Damjanovic, M. Gureev, and N. Setter, Enhanced electromechanical response of ferroelectrics due to charged domain walls, Nat. Commun. **3**, 748 (2012).

[11] O. Condurache, G. Dražić, N. Sakamoto, T. Rojac, and A. Benčan, Atomically resolved structure of step-like uncharged and charged domain walls in polycrystalline BiFeO 3, J. Appl. Phys. **129**, 054102 (2021).

[12] T. Rojac, A. Bencan, G. Drazic, N. Sakamoto, H. Ursic, B. Jancar, G. Tavcar, M. Makarovic, J. Walker, B. Malic, and D. Damjanovic, Domain-wall conduction in ferroelectric $BiFeO_3$ controlled by accumulation of charged defects, Nat. Mater. **16**, 322 (2017).

[13] I. Stolichnov, L. Feigl, L. J. McGilly, T. Sluka, X.-K. Wei, E. Colla, A. Crassous, K. Shapovalov, P. Yudin, A. K. Tagantsev, and N. Setter, Bent ferroelectric domain walls as reconfigurable metallic-like channels, Nano Lett. **15**, 8049 (2015).

[14] T. Sluka, A. K. Tagantsev, P. Bednyakov, and N. Setter, Free-electron gas at charged domain walls in insulating BaTiO3, Nat. Commun. **4**, 1808 (2013).

[15] W. Wu, Y. Horibe, N. Lee, S.-W. Cheong, and J. R. Guest, Conduction of Topologically Protected Charged Ferroelectric Domain Walls, Phys. Rev. Lett. **108**, 077203 (2012).

[16] J. Gonnissen, D. Batuk, G. F. Nataf, L. Jones, A. M. Abakumov, S. Van Aert, D. Schryvers, and E. K. H. Salje, Direct observation of ferroelectric domain walls in $LiNbO_3$: Wall-meanders, kinks, and local electric charges, Adv. Funct. Mater. **26**, 7599 (2016).

[17] C. S. Werner, S. J. Herr, K. Buse, B. Sturman, E. Soergel, C. Razzaghi, and I. Breunig, Large and accessible conductivity of charged domain walls in lithium niobate, Sci. Rep. **7**, 9862 (2017).

[18] M. Schröder, A. Haußmann, A. Thiessen, E. Soergel, T. Woike, and L. M. Eng, Conducting domain walls in lithium niobate single crystals, Adv. Funct. Mater. **22**, 3936 (2012).

[19] C. Godau, T. Kämpfe, A. Thiessen, L. M. Eng, and A. Haußmann, Enhancing the domain wall conductivity in lithium niobate single crystals, ACS Nano **11**, 4816 (2017).

[20] H. Lu, Y. Tan, J. P. V. McConville, Z. Ahmadi, B. Wang, M. Conroy, K. Moore, U. Bangert, J. E. Shield, L. Chen, J. M. Gregg, and A. Gruverman, Electrical tunability of domain wall conductivity in $LiNbO_3$ thin films, Adv. Mater. **31**, 1902890 (2019).

[21] Z. Chen, X. Zou, W. Ren, L. You, C. Huang, Y. Yang, P. Yang, J. Wang, T. Sritharan, L. Bellaiche, and L. Chen, Study of strain effect on in-plane polarization in epitaxial BiFeO 3 thin films using planar electrodes, Phys. Rev. B **86**, 235125 (2012).

[22] A. Alsubaie, P. Sharma, G. Liu, V. Nagarajan, and J. Seidel, Mechanical stress-induced switching kinetics of ferroelectric thin films at the nanoscale, Nanotechnology **28**, 075709 (2017).

[23] C. Ederer and N. A. Spaldin, Effect of Epitaxial Strain on the Spontaneous Polarization of Thin Film Ferroelectrics, Phys. Rev. Lett. **95**, 257601 (2005).

[24] D. Chen, Z. Bai, Y. Zhang, and A. Jiang, Strain induced enhancement of erasable domain wall current in epitaxial $BiFeO_3$ thin films, J. Appl. Phys. **124**, 194102 (2018).

[25] D. G. Schlom, L.-Q. Chen, C.-B. Eom, K. M. Rabe, S. K. Streiffer, and J.-M. Triscone, Strain tuning of ferroelectric thin films, Annu. Rev. Mater. Res. **37**, 589 (2007).

[26] C. W. Hicks, M. E. Barber, S. D. Edkins, D. O. Brodsky, and A. P. Mackenzie, Piezoelectric-based apparatus for strain tuning, Rev. Sci. Instrum. **85**, 065003 (2014).

[27] M. Müller, E. Soergel, and K. Buse, Influence of ultraviolet illumination on the poling characteristics of lithium niobate crystals, Appl. Phys. Lett. **83**, 1824 (2003).

[28] M. C. Wengler, U. Heinemeyer, E. Soergel, and K. Buse, Ultraviolet light-assisted domain inversion in magnesium-doped lithium niobate crystals, J. Appl. Phys. **98**, 064104 (2005).

[29] T. Kämpfe, P. Reichenbach, M. Schröder, A. Haußmann, L. M. Eng, T. Woike, and E. Soergel, Optical three-dimensional profiling of charged domain walls in ferroelectrics by Cherenkov second-harmonic generation, Phys. Rev. B **89**, 035314 (2014).

[30] See Supplemental Material at http://link.aps.org/supplemental/10.1103/PhysRevB.106.144103 for details on the domain wall conductivity enhancement and domain wall angle calculations in Sec. S1, calculations on piezoelectricity based model in Sec. S2, supplemental results such as intermediate cAFM scans, long-term and short-term stability in Sec. S3.

[31] E. Soergel, Piezoresponse force microscopy (PFM), J. Phys. D **44**, 464003 (2011).

[32] T. Yamada, N. Niizeki, and H. Toyoda, Piezoelectric and elastic properties of lithium niobate single crystals, Jpn. J. Appl. Phys. **6**, 151 (1967).

[33] R. T. Smith and F. S. Welsh, Temperature dependence of the elastic, piezoelectric, and dielectric constants of lithium tantalate and lithium niobate, J. Appl. Phys. **42**, 2219 (1971).

[34] R. S. Weis and T. K. Gaylord, Lithium niobate: Summary of physical properties and crystal structure, Appl. Phys. A: Solids Surf. **37**, 191 (1985).

[35] S. H. Wemple, M. DiDomenico, and I. Camlibel, Relationship between linear and quadratic electrooptic coefficients in $LiNbO_3$, $LiTiO_3$, and other oxygen octahedra ferroelectrics based on direct measurement of spontaneous polarization, Appl. Phys. Lett. **12**, 209 (1968).

[36] S. Y. Xiao, T. Kämpfe, Y. M. Jin, A. Haußmann, X. M. Lu, and L. M. Eng, Dipole-Tunneling Model from Asymmetric Domain-Wall Conductivity in $LiNbO_3$ Single Crystals, Phys. Rev. Appl. **10**, 034002 (2018).

[37] B. Wolba, J. Seidel, C. Cazorla, C. Godau, A. Haußmann, and L. M. Eng, Resistor network modeling of conductive domain walls in lithium niobate, Adv. Electron. Mater. **4**, 1700242 (2018).

[38] E. A. Eliseev, A. N. Morozovska, G. S. Svechnikov, V. Gopalan, and V. Y. Shur, Static conductivity of charged domain walls in uniaxial ferroelectric semiconductors, Phys. Rev. B **83**, 235313 (2011).

[39] www.FOR5044.de